

Article

Experimental Study on the Separation of Selected Metal Elements (Sm, Co, Fe, and Cu) from Nitric Acid Leachate Using Specific Precipitants

Jian-Zhi Wang^{1,2,*}, Yi-Chin Tang^{1,3} and Yun-Hwei Shen¹ 

¹ Department of Resources Engineering, National Cheng Kung University, Tainan 70101, Taiwan; n48091500@gs.ncku.edu.tw (Y.-C.T.); yhshen@mail.ncku.edu.tw (Y.-H.S.)

² Department of Mechanical Engineering, National Kaohsiung University Science and Technology, No. 415, Jiangong Rd, Kaohsiung 80778, Taiwan

³ Green Energy and System Integration Research and Development Department, China Steel Corporation, Kaohsiung 81233, Taiwan

* Correspondence: n48091518@gs.ncku.edu.tw; Tel.: +886-979884436

Abstract: As more countries emphasize the importance of the circular economy, recycling resources from waste has become increasingly crucial. This study proposes a novel separation process for SmCo magnets, which can separate and recover metals by precipitation, thus reducing the amount of solvent used. The precipitation process involved the use of Na₂SO₄, NH₄OH, and H₂C₂O₄ to separate Sm, Fe, Cu, and Co, resulting in high precipitation efficiencies of 96.11%, 99.97%, 93.81%, and 98.15%, respectively. Moreover, the recovered metals can be directly used to create magnets after calcination, making this process a step towards achieving a circular economy.

Keywords: SmCo magnet; precipitation; resource recovery; recycling



Citation: Wang, J.-Z.; Tang, Y.-C.; Shen, Y.-H. Experimental Study on the Separation of Selected Metal Elements (Sm, Co, Fe, and Cu) from Nitric Acid Leachate Using Specific Precipitants. *Recycling* **2024**, *9*, 111. <https://doi.org/10.3390/recycling9060111>

Academic Editor: Ana Paula Paiva

Received: 14 October 2024

Revised: 10 November 2024

Accepted: 12 November 2024

Published: 14 November 2024



Copyright: © 2024 by the authors. Licensee MDPI, Basel, Switzerland. This article is an open access article distributed under the terms and conditions of the Creative Commons Attribution (CC BY) license (<https://creativecommons.org/licenses/by/4.0/>).

1. Introduction

Rare earth elements include light rare earth elements (LREEs) such as Lanthanum (La), Cerium (Ce), Praseodymium (Pr), Neodymium (Nd), Promethium (Pm), Samarium (Sm), and Europium (Eu), and heavy rare earth elements (HREEs) such as Gadolinium (Gd), Terbium (Tb), Dysprosium (Dy), Holmium (Ho), Erbium (Er), Thulium (Tm), Ytterbium (Yb), and Lutetium (Lu). Yttrium (Y) and Scandium (Sc) are two other elements excluded from the LREEs and HREEs classifications [1,2]. The Sm in SmCo magnets belongs to the light rare earth elements.

In 2022, the global rare earth reserves amounted to approximately 130 million metric tons. Among them, China, Vietnam, Brazil, and Russia hold 44 million, 22 million, 21 million, and 21 million metric tons of rare earth reserves, respectively [3]. These four countries together possess more than 80% of the world's rare earth reserves. Rare earth reserves are excessively concentrated in specific countries. In addition, the production of rare earth is also concentrated in specific countries. China's rare earth production in 2022 was 210,000 metric tons, which represented about 70% of the total global rare earth production [3]. Furthermore, in 2010, China issued the "The Opinion on Promoting Mergers and Acquisitions of Enterprises" [4], which listed rare earth elements as a key industry for mergers, acquisitions, and reorganization, in an attempt to reduce the export of rare earths. This led to a historical high in the price of rare earths [5]. The most effective method currently to reduce the risk of rare earth supply is to recycle metals from waste [6,7].

Rare earth elements have become a significant topic of discussion among researchers, entrepreneurs, and politicians in recent years due to their crucial role in current technological advancements. Rare earths are utilized in a broad range of applications [8–10], including wind turbines, electric vehicles [11], mobile phones, hard disk drives, fluorescent and LED lamps, defense applications, catalysts, pharmaceuticals, and medicine [12]. Of

these, over a quarter of rare earths are utilized in magnet manufacturing [13], which is the field that consumes the most rare earths. Consequently, if a large number of magnets can be recycled, rare earth elements can be effectively recovered.

Among the rare earth elements, Nd and Sm are commonly used in magnet production. Nd is primarily used to create NdFeB magnets, which are widely applied across industries due to their high energy density. These industries include acoustic transducers, wind turbines, electric vehicles, industrial motors, missiles, tanks, warplanes, submarines, microwaves, computers, printers, and hard disk drives [14–16]. In comparison, SmCo magnets exhibit unique properties, including higher coercivity and superior temperature resistance, making them ideal for specialized applications like aero engines [17–19]. While NdFeB magnets currently account for over 90% of annual rare earth magnet production, many experts predict an increase in demand for SmCo magnets in the coming years [20]. This shift is largely due to the high cost of dysprosium (Dy), a key component in NdFeB magnets. Consequently, innovative direct and indirect recycling methods for SmCo magnets must be developed.

Currently, methods for recovering rare earth from NdFeB magnets include hydrometallurgical processes [21–24] and pyrometallurgical processes [25–28]. However, there have been few studies on the recovery of rare earths from SmCo magnets. In the literature [29–31] on the pre-treatment of SmCo magnets, waste magnets were first demagnetized in a high-temperature furnace. Sinha et al. (2017) [29] proposed demagnetizing them at a temperature of 850 °C for 6 h. Then, SmCo magnets should be crushed and ground using a hydraulic press and grinder, which is beneficial for follow-up research. Sinha et al. (2017) [29] also suggested mechanically crushing, grinding, and screening the SmCo magnet ring with a 150 µm sieve. After completing the pretreatment process, most studies [29,31–33] use hydrometallurgical methods to purify and separate valuable metals. First, the powder is leached with either an inorganic acid (such as sulfuric acid, hydrochloric acid, or nitric acid) [29,31,32] or an organic acid (such as citric acid) [34]. However, Zhou et al. [33] (2017) proposed using sulfuric acid to leach waste SmCo magnets. Unfortunately, Sm easily reacts with sulfuric acid to form samarium sulfate precipitation, which results in poor leaching efficiency. Therefore, most studies [29,32] have used hydrochloric acid and nitric acid for leaching. After the leaching experiment was completed, the study used solvent extraction [17,29,32,35], ion exchange [36], and precipitation [31,33,37,38] methods for metal separation. Finally, the recovered powder was calcined to meet the raw materials for making magnets. Sahoo et al. proposed that the separated Sm and Co solutions be precipitated with oxalic acid, and then the samarium oxalate and cobalt oxalate were calcined at 800 °C and 450 °C, respectively, to form metal oxides.

One of the primary strategies for circulating magnet materials throughout the supply chain involves proposing the most effective approach to refine valuable materials from discarded SmCo magnets. However, the above studies [17,29,31–33,35,37,38] only focused on the recovery of Sm and Co, and did not purify and separate all metals (Sm, Co, Fe, Cu, and Zr) in the waste. Therefore, this study hopes to propose a complete recovery method to deal with real waste. In addition, in the separation method, after the metal is separated by the solvent extraction method, metal precipitation is required, and the process is relatively complicated. The ion exchange method, on the other hand, requires diluting the aqueous solution, resulting in increased wastewater volumes. In this study, a simpler process was developed, using the precipitation method to directly separate the metal by precipitation, so the metal could be reprocessed into a magnet.

2. Results and Discussion

2.1. Selective Precipitation of Sm by Na_2SO_4

To facilitate subsequent research, precipitation experiments were carried out using a $L_9(3^4)$ orthogonal table to determine the precipitation efficiency of Sm. The results of these experiments, showing the precipitation efficiencies of Sm under different parameters,

are presented in Table 1. The precipitation efficiency was observed to be affected by the temperature, addition of Na_2SO_4 , and time [33].

Table 1. The orthogonal array experiment results of Sm precipitation.

No.	Temp.	Time	Na_2SO_4	Sm	Co	Fe	Cu
Unit	$^{\circ}\text{C}$	min	(w/v)%	%	%	%	%
1	70	20	6	17.69	0.09	0.64	0
2	70	40	9	90.88	2.05	3.51	1.13
3	70	60	12	99.19	2.31	6.06	0.88
4	80	20	9	90.22	1.78	5.74	0.84
5	80	40	12	99.31	2.85	4.31	0.84
6	80	60	6	44.63	1.25	2.71	0
7	90	20	12	99.40	3.03	4.78	1.34
8	90	40	6	48.59	0	0	0
9	90	60	9	95.60	0	3.19	0

In this study, the priority of each factor on Sm precipitation efficiency was analyzed through factor effect analysis using results from orthogonal table experiments. The precipitation efficiency at the addition of Na_2SO_4 of K3 (as shown in Table 2) represents the average precipitation efficiency with an addition of Na_2SO_4 of 12 (w/v)% (as shown in Table 1). The extreme deviation is the difference between the best and worst precipitation rates of Sm under K1 to K3 conditions. The order of priority for factors that affect precipitation efficiency was determined using extreme deviation [39,40].

Table 2. Factor response table for Sm precipitation.

	Effect Factor	Temperature	Time	Na_2SO_4
Sm	K1	69.25%	69.10%	36.97%
	K2	78.05%	79.60%	92.23%
	K3	81.20%	79.81%	99.30%
	Extreme Deviation	11.94%	10.70%	62.33%
Priority Order		$\text{Na}_2\text{SO}_4 > \text{Temperature} > \text{Time}$		

Table 2 shows the factor response table for the precipitation rate, which revealed that the order of influence on precipitation efficiency was $\text{Na}_2\text{SO}_4 > \text{temperature} > \text{time}$. The preliminary optimal parameters determined were 12 (w/v)% Na_2SO_4 addition, 80 $^{\circ}\text{C}$ temperature, and 40 min time, which resulted in the highest precipitation efficiency. As the precipitation efficiency at 40 and 60 min was found to be equivalent, 40 min was chosen as the initial optimum parameter. Similarly, as the precipitation efficiency at 80 and 90 $^{\circ}\text{C}$ was also found to be equivalent, 80 $^{\circ}\text{C}$ was selected as the initial optimum parameter time.

Figure 1 illustrates the results of the Sm precipitation confirmation experiment. As shown in Figure 1a, Sm precipitation efficiency was less than 50% when 6 (w/v)% of sodium sulfate was added. However, when the amount of sodium sulfate was increased to 10 (w/v)%, the precipitation efficiency of Sm significantly improved, reaching 96.25%. Therefore, the amount of sodium sulfate added was identified as the most crucial parameter, as it had a significant impact on precipitation effectiveness.

Compared with the amount of sodium sulfate added, the temperature had a negligible effect on Sm precipitation efficiency, as depicted in Figure 1b. When the Sm temperature was 60 $^{\circ}\text{C}$, the precipitation efficiency reached 93.44%, and increasing the temperature did not result in a significant improvement in precipitation efficiency. However, at a temperature of 60 $^{\circ}\text{C}$, the co-precipitation efficiency of Fe was 18.56%. Thus, 60 $^{\circ}\text{C}$ was not the optimal precipitation parameter. The primary reason for Fe co-precipitation was

that Fe readily forms ferric sulfate precipitation at lower temperatures [41–43], resulting in increased co-precipitation rates of Fe. Therefore, the optimal temperature was 70 °C.

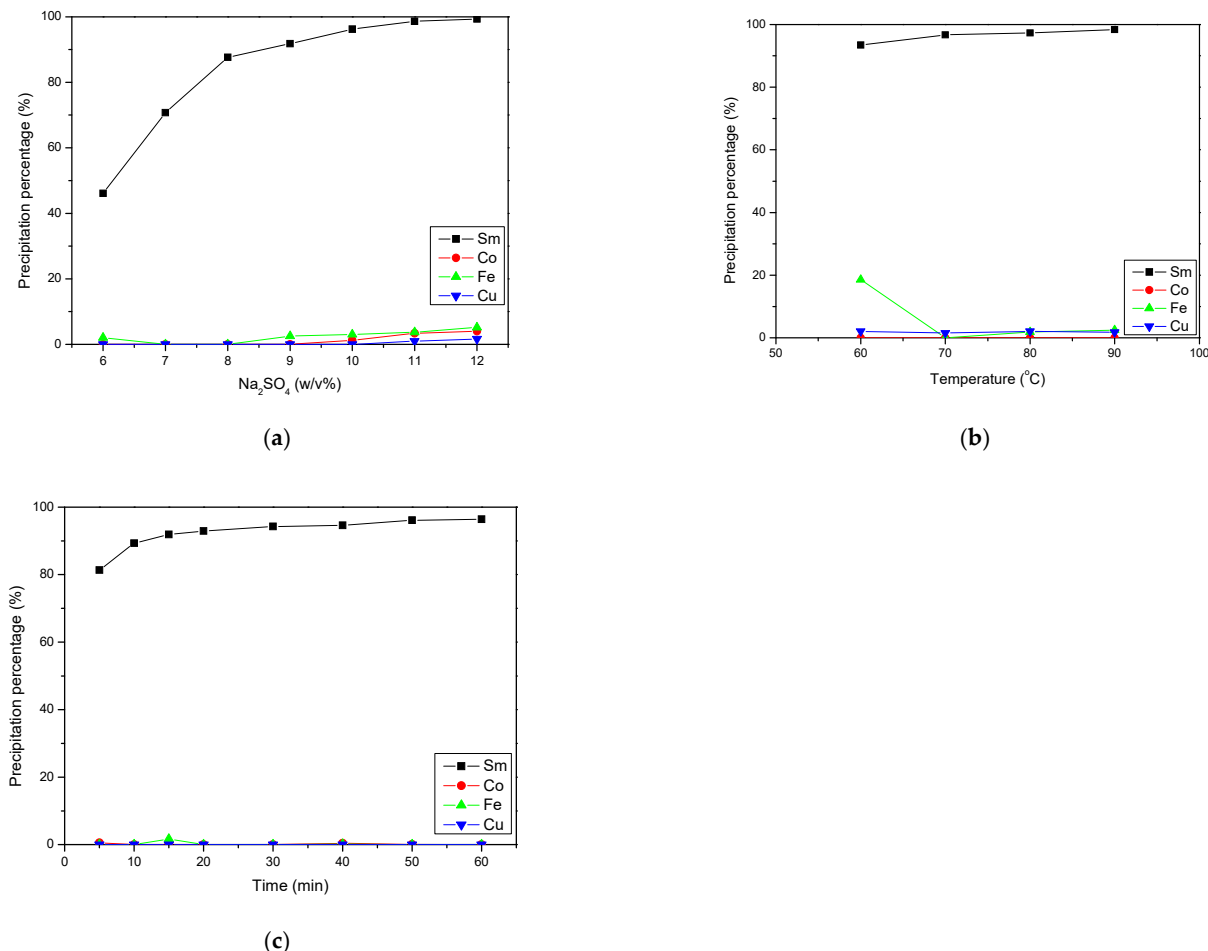


Figure 1. Effects of (a) addition of sodium sulfate (temperature = 80 °C, time = 40 min), (b) temperature ([Na₂SO₄] = 10 (w/v)%, time = 40 min), and (c) time ([Na₂SO₄] = 10 (w/v)%, temperature = 70 °C) on Sm precipitation.

Figure 1c shows that the Sm precipitation reaction was relatively slow, and it took 50 min to achieve a Sm precipitation rate higher than 95%.

Combining the above results, the optimal conditions for precipitation were determined to be the addition of 10 (w/v)% of sodium sulfate, a temperature of 70 °C, and a precipitation time of 50 min. Under these conditions, the precipitation rates of Sm, Co, Fe, and Cu were 96.11%, 0.05%, 0%, and 0%, respectively. This successful separation of Sm resulted in a co-precipitation rate of other metals that were less than 0.1%.

The findings of this study were compared to those of Zhou et al. [33] (Table 3). Zhou et al. [33] utilized sulfuric acid for leaching, resulting in a solution with a high concentration of sulfate ions, which promoted the precipitation of sodium samarium bisulfate. Consequently, less sodium sulfate was added in their study. The precipitation of sodium samarium bisulfate is demonstrated in Formula (1). Despite the higher molar ratio used in this study, a greater amount of Sm was successfully precipitated at lower temperature and time conditions. Moreover, this study effectively optimized the parameters for Sm precipitation.



Table 3. Comparison of results for Sm precipitation.

No.	This Study	Zhou et al. [33]
Temp.	70 °C	80 °C
Time	50 min	60 min
Molar ratio	6.69:1	4:1
Leachate	HNO ₃	H ₂ SO ₄
Ions in the leachate	Sm, Co, Fe, and Cu	Sm and Co
The precipitation rate of Sm	96.11%	93.4%

2.2. Selective Precipitation of Fe by NaOH

This section analyzes the impact of pH and time on Fe precipitation. Figure 2a shows the effect of pH on Fe precipitation, revealing that the efficiency of Fe precipitation was less than 10% when the pH was below 2.5, and the co-precipitation rate of Cu exceeded 50% when the pH was above 4. Thus, pH was a crucial factor in Fe precipitation. The optimal Fe precipitation rate of 98.28% was achieved at a pH of 3.5, with less than 1% co-precipitation of other metals. Therefore, a pH of 3.5 was selected as the optimal parameter.

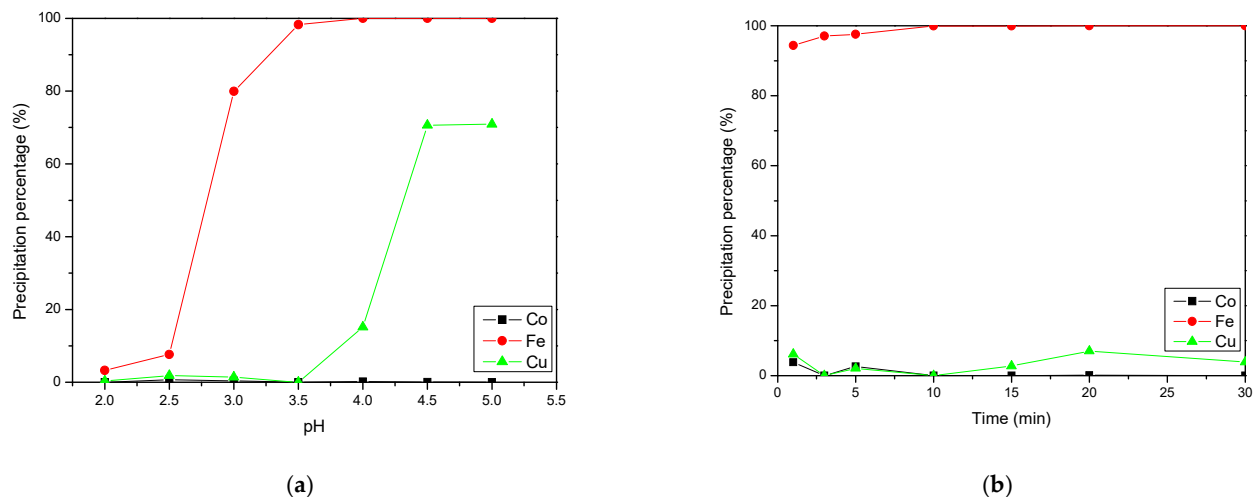


Figure 2. Effects of (a) pH (temperature = 25 °C, time = 60 min) and (b) time (pH = 3.5, temperature = 25 °C) on Fe precipitation.

The results regarding the effect of time on Fe precipitation are shown in Figure 2b. The efficiency of Fe precipitation was faster compared with that of Sm precipitation. At a time of 10 min, the precipitation rate of Fe reached 99.97%.

Combining the aforementioned results, it can be concluded that the precipitation rates of Fe, Cu, and Co were 99.97%, 0%, and 0%, respectively, when the pH was 3.5 and the time was 10 min. Fe was successfully separated, and the co-precipitation rate of other metals was less than 0.1%.

The study of SmCo magnets has not yielded any other studies on Fe precipitation separation so far. Therefore, no comparison of experimental results was made, highlighting the novelty of this study.

2.3. Selective Precipitation of Cu by NaOH

This section discusses the impact of pH and time on the efficiency of Cu precipitation. The effect of pH on the Cu precipitation efficiency is demonstrated in Figure 3a. The pH level played a crucial role in Cu precipitation as it significantly influenced precipitation efficiency. The optimal precipitation pH value was found to be 6.5, resulting in a Cu precipitation efficiency of 94.93%.

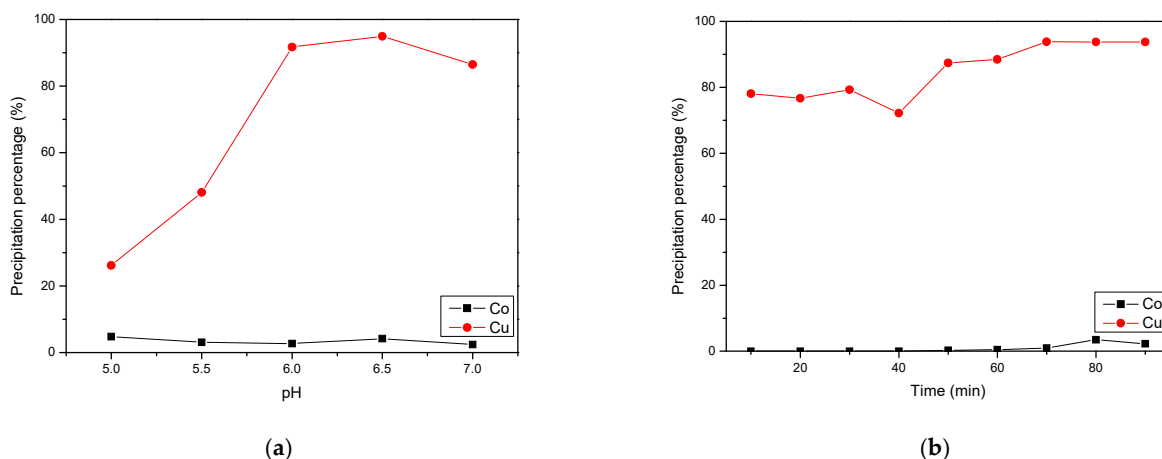


Figure 3. Effects of (a) pH (temperature = 25 °C, time = 60 min) and (b) time (pH = 6.5, temperature = 25 °C) on Cu precipitation.

Figure 3b shows the effect of time on Cu precipitation efficiency. The Cu precipitation rate was slow, taking more than 70 min to achieve over 90% efficiency.

By combining the above findings, it was determined that a pH of 6.5 and a precipitation time of 70 min resulted in Cu and Co precipitation rates of 93.81% and 0.95%, respectively, indicating successful Cu separation with less than 1% Co co-precipitation.

The study of SmCo magnets has not yielded any other studies on Cu precipitation separation so far. Therefore, no comparison of experimental results was made, highlighting the novelty of this study.

2.4. Selective Precipitation of Co by Oxalic Acid

This part discusses the influence of molar ratio and time on the Co precipitation effect, as shown in Figure 4. As the molar ratio increased from 0.5 to 1.5, the Co precipitation efficiency increased from 76.76% to 96.84%. However, increasing the precipitation time did not significantly increase the precipitation efficiency. Therefore, the molar ratio had a greater influence on Co precipitation.

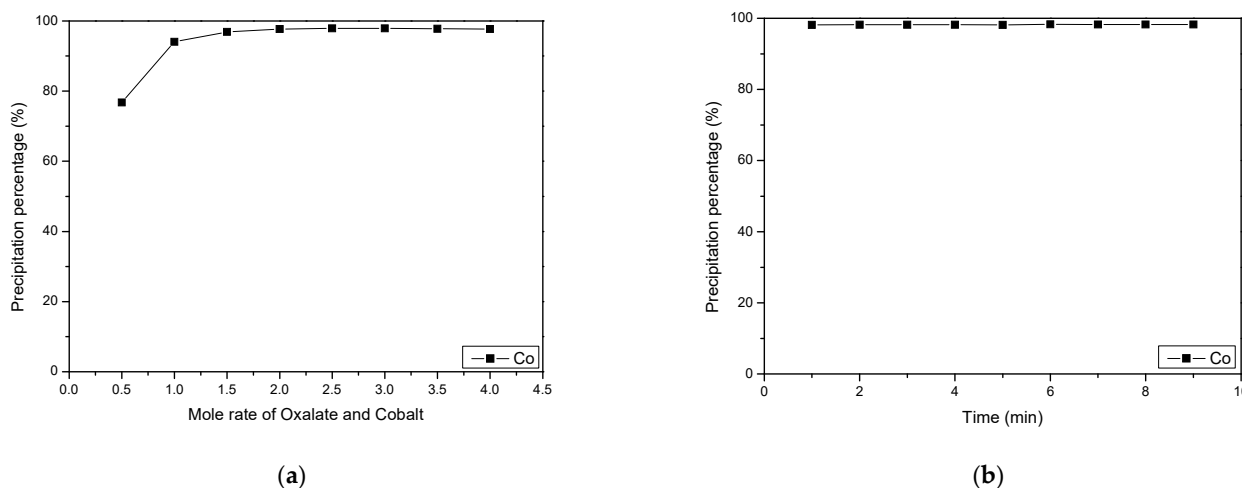


Figure 4. Effects of (a) molar ratio (temperature = 25 °C, time = 60 min) and (b) time (molar ratio = 1.5, temperature = 25 °C) on Co precipitation.

In the study of the influence of time on Co precipitation, it was found that the Co precipitation rate was very fast. The Co precipitation efficiency reached 98.15% in 1 min.

Based on the above results, the precipitation rate of Co reached 98.15% under the condition of a molar ratio of 1.5 and a time of 1 min. These results were compared with

those of Wang et al. [36] (Table 4). Despite the higher molar ratio used in this study, more Co was successfully precipitated under lower temperature and time conditions. Moreover, this study effectively optimized the parameters for Co precipitation.

Table 4. Comparison of results for Co precipitation.

No.	This Study	Wang et al. [36]
Temp.	25 °C	60 °C
Time	1 min	60 min
Molar ratio	1.5:1	1:1
Leachate	HNO ₃	H ₂ SO ₄
The precipitation rate of Co	98.15%	96.20%

2.5. Characterization of NaSm(SO₄)₂

As NaSm(SO₄)₂ releases sulfur oxides during TGA analysis, which can damage the instrument, the oxidation temperature was not determined. However, Denisenko et al. [44] proposed that heating NaSm(SO₄)₂ to 1187 °C would decompose it into liquid sodium sulfate and solid samarium oxide. In this study, NaSm(SO₄)₂ can be used to obtain samarium oxide, which can be reused to make magnets.

The Sm precipitate obtained was analyzed by XRD, and the results are displayed in Figure 5. The major peaks of NaSm(SO₄)₂ · H₂O at 25.699°, 29.736°, 42.325°, and 49.278° were observed, confirming the presence of crystalline NaSm(SO₄)₂ · H₂O as the dominant phase.

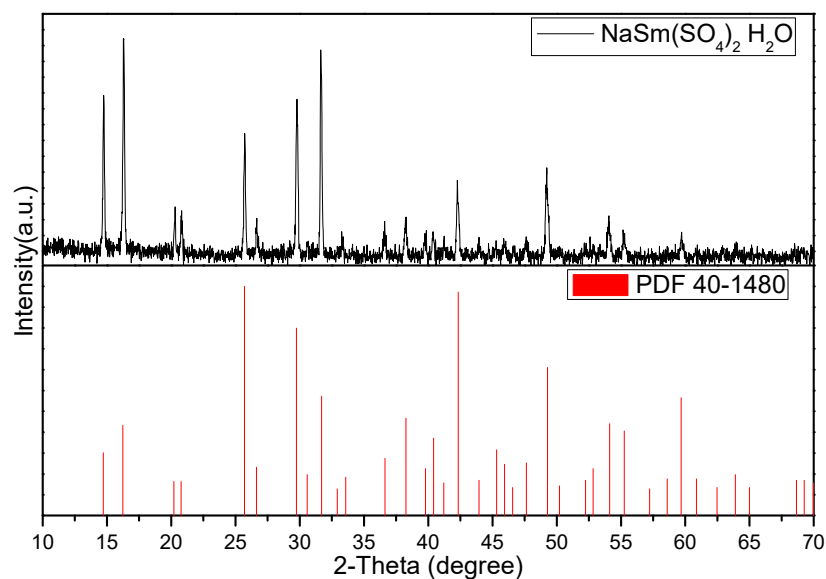


Figure 5. The XRD analysis of NaSm(SO₄)₂.

2.6. Preparation of Iron Oxide and Characterization

The TGA diagram and oxidation formula of Fe(OH)₃ are shown in Figure 6a and Formula (2), respectively. It can be observed that there is no significant weight loss when the temperature reached 500 °C, and the weight remained at about 59.40% of the original weight. Based on the theory of weight loss after oxidation, it can be concluded that the final oxidation temperature of Fe(OH)₃ was 500 °C.

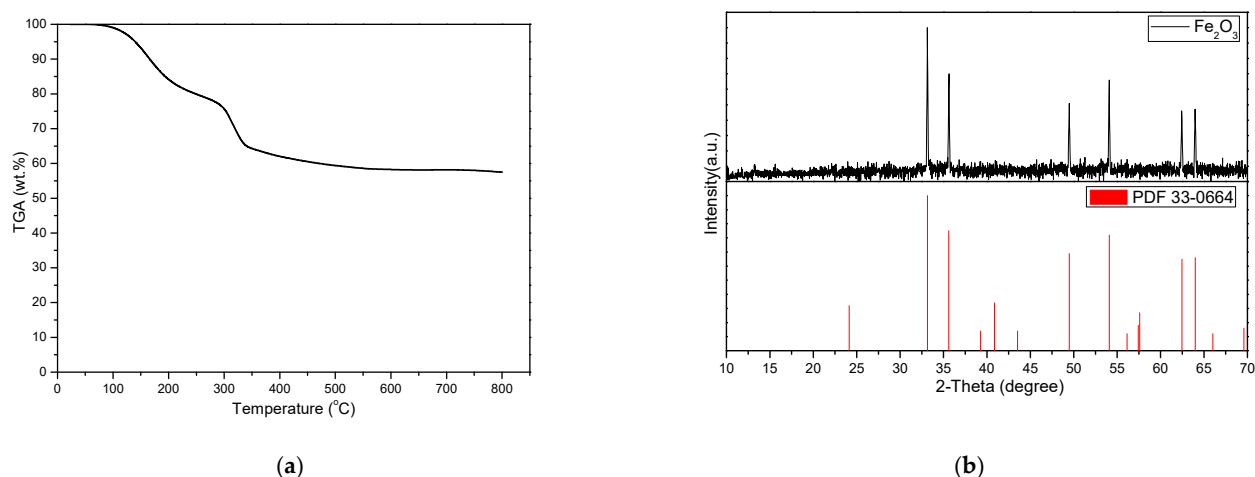


Figure 6. The (a) TGA analysis of Fe(OH)₃ and the (b) XRD analysis of Fe₂O₃.

Fe(OH)₃ was calcined at 500 °C for 4 h, and the XRD analysis was performed (Figure 6b). The results showed that after calcination, the sample exhibited the main peak of Fe₂O₃ at 33.152°, confirming that Fe(OH)₃ had transformed into Fe₂O₃.



2.7. Preparation of Copper Oxide and Characterization

Figure 7a and Formula (3) depict the TGA diagram and oxidation formula of Cu(OH)₂, respectively. Upon analysis, it was observed that there was no significant weight loss when the temperature reached 500 °C. At this temperature, the weight was approximately 80.36% of the original weight, which was consistent with the theoretical value of weight loss after oxidation. Thus, 500 °C was determined to be the final oxidation temperature of Cu(OH)₂.

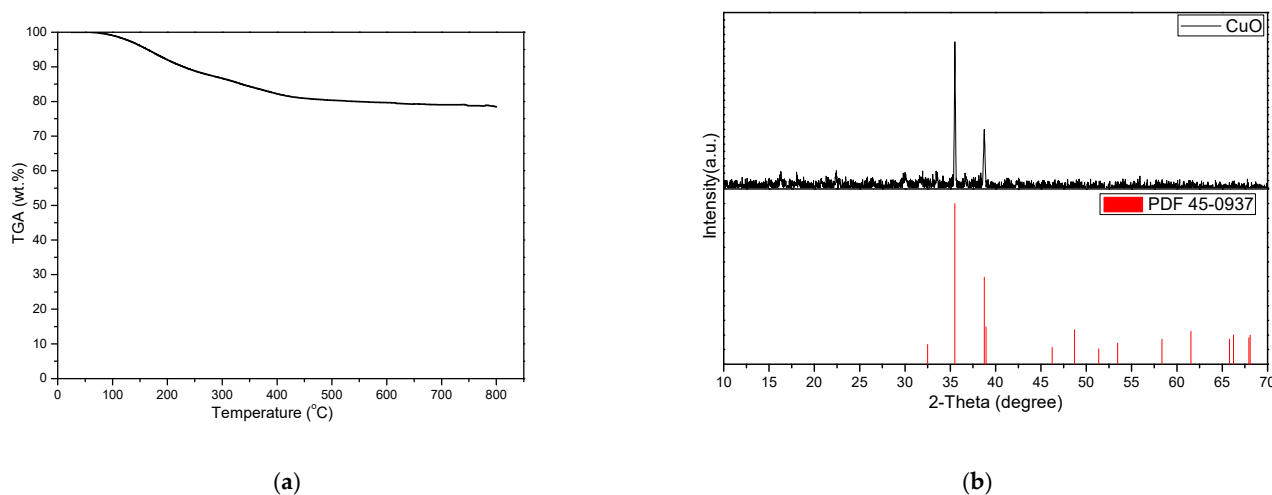


Figure 7. The (a) TGA analysis of Cu(OH)₂ and the (b) XRD analysis of CuO.

After calcining Cu(OH)₂ at 500 °C for 4 h, the XRD analysis was performed, and the results are shown in Figure 7b. The XRD pattern of the calcined Cu(OH)₂ matches with the main peaks of CuO at 35.495° and 38.730°, confirming the transformation of Cu(OH)₂ to CuO upon calcination.



2.8. Preparation of Cobalt Oxide and Characterization

The TGA diagram and oxidation formula of CoC_2O_4 are shown in Figure 8a and Formula (4), respectively. Upon analysis, it was observed that there was no significant weight loss when the temperature reached 470 °C. At this temperature, the weight was approximately 38.98% of the original weight, which was consistent with the theoretical value of weight loss after oxidation. Therefore, 470 °C was determined to be the oxidation temperature of CoC_2O_4 .

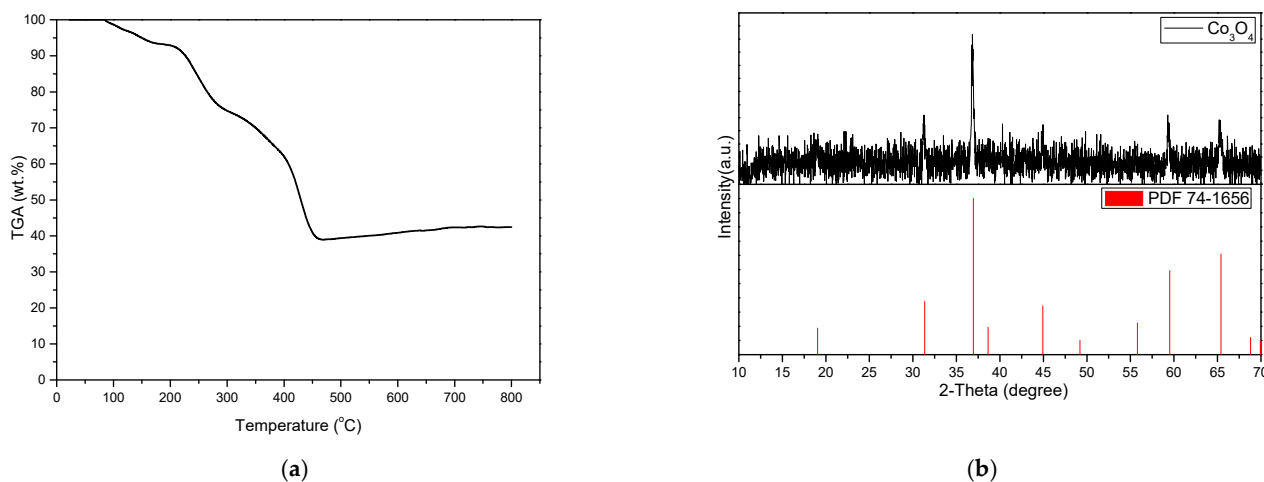


Figure 8. The (a) TGA analysis of CoC_2O_4 and the (b) XRD analysis of Co_3O_4 .

After calcination of CoC_2O_4 at 500 °C for 4 h, the XRD analysis was performed, and the results are shown in Figure 8b. The XRD pattern of the calcined CoC_2O_4 corresponds to the main peaks of Co_3O_4 at 36.935°, 59.508°, and 65.406°, confirming the transformation of CoC_2O_4 to Co_3O_4 upon calcination.



3. Materials and Methods

3.1. Materials

Tai Chuan Metal Co., Ltd. (Taipei, Taiwan) provided the SmCo magnet scraps used in this study, which were abundant in Sm, Co, Fe, Cu, and Zr. Table 5 displays the composition of the SmCo magnet scrap after digestive analysis and the concentrations of Sm, Co, Fe, and Cu in the leachate, which only contains these metals since Zr, which cannot be leached [45], was initially separated during the leaching process. The leachate was produced at a temperature of 25 °C, a nitric acid concentration of 2.5 mol L⁻¹, a solid-to-liquid ratio of 65 g L⁻¹, and a time of 1 min, resulting in a leaching efficiency of 99.52%, 92.45%, 92.84%, and 94.30% for Sm, Co, Fe, and Cu, respectively.

Table 5. The content of the SmCo magnet and the concentration in the leachate.

Element	Sm	Co	Fe	Cu	Zr
The weight percent of element (wt.%)	22.70	51.08	14.51	5.12	4.31
Metal concentration in leachate (ppm)	15,756	31,088	8762	3174	-

Nitric acid (HNO_3 , 70%) and hydrochloric acid (HCl , 37%) for aqua regia digestion, nitric acid (HNO_3 , 70%) for leaching, sodium sulfate (Na_2SO_4 , 99.5%) for Sm precipitation, ammonia (NH_4OH , 29%) for precipitation of Fe and Cu, and oxalic acid ($\text{H}_2\text{C}_2\text{O}_4$, 99%)

for Co precipitation were purchased from Echo Chemical Co., Ltd. (Miaoli, Taiwan). All aqueous solutions were prepared in deionized water.

3.2. Equipment

The pH of the solution was monitored by a pH meter (PL-700PVS, Dogger Science, Taipei, Taiwan). In order to control the precipitation and leaching temperature, the precipitation and leaching process was carried out in a thermostatic bath with magnetic stirring (Shin-Kwang Precision Industry Ltd., New Taipei, Taiwan). Subsequently, the solid–liquid separation was carried out through a filter device (Chemker 300, Rone Scientific Co., Ltd., New Taipei, Taiwan). An atomic absorption spectrometer (AAS, PinAAcle 900F AA Spectrometer, PerkinElmer Inc., Waltham, MA, USA) was used to analyze the concentration of metals in the aqueous solution. The oxidation temperature of Fe(OH)₃, Cu(OH)₂, and CoC₂O₄ in the precipitation were analyzed by thermogravimetry analysis (TGA, TGA-51, Shimadzu, Japan). The crystal structure of the product (NaSm(SO₄)₂, Fe₂O₃, CuO, and Co₃O₄) were analyzed via X-ray diffractometry (XRD, DX-2600, Dandong, China), with Cu K α radiation ranging from $2\theta = 10\text{--}70^\circ$, to identify the phases present. The precipitate was calcined using a high-temperature furnace (Thermo Scientific Lindberg/Blue M BF51866C Muffle Furnace, Hogentogler & Co., Inc., Howard County, Columbia, MD, USA).

3.3. Experimental Method

3.3.1. The Composition of the Magnet

To confirm the powder composition, aqua regia digestion was utilized. In detail, 1 g of SmCo magnet powder was added to a 250 mL conical flask containing 10 mL of nitric acid and 30 mL of hydrochloric acid. The flask was then placed in a thermostatic bath at 90 °C for one day to guarantee complete metal dissolution. The metal concentration in the resulting aqueous solution was analyzed using AAS. The contents of Sm, Co, Fe, Cu, and Zr in the magnet are displayed in Table 5.

3.3.2. Leaching of Magnets

The hydrometallurgical method was employed in this study to recover the metals from the magnet. For leaching, SmCo magnet powder and 100 mL of an acid solution (a mixture of deionized water and the required amount of acid) were added to a 250 mL conical flask, and the experimental temperature was regulated using a thermostatic bath. The resulting solution was filtered, and the metal concentration was analyzed using AAS. The leaching efficiency (L%) was determined using Formula (5) [33].

$$L(\%) = \frac{V_1(L) \times C_1(\text{g L}^{-1})}{M_1(\text{g}) \times W_1} \times 100\% \quad (5)$$

where M_1 is the mass of the alloy sample, W_1 is the metal content of the alloy sample, V_1 is the volume of the leach solution, and C_1 is the mass concentration of the metal in the leach solution.

3.3.3. Precipitation Method

For the precipitation experiment, this study added 100 mL of leachate and precipitant to a 250 mL Erlenmeyer flask. The experimental temperature and stirring rate were controlled using a thermostatic bath. The resulting solution was filtered, and the metal concentration was analyzed using AAS. The precipitation efficiency (P%) was determined using Formula (6) [33].

$$P\% = \frac{V_2 \times C_2 - V_3 \times C_3}{V_2 \times C_3} \times 100\% \quad (6)$$

where P is the precipitation percentage of metal, V_2 and V_3 are the volume of the leachate and the filtrate, respectively, and C_2 and C_3 are the mass concentrations of metal in the leachate and in the filtrate, respectively.

3.3.4. Sm Precipitation

The previous study [33] revealed that sodium sulfate exhibited selective separation characteristics for Sm precipitation under low pH conditions. Therefore, this study first employed sodium samarium sulfate to investigate Sm separation. In contrast to the study by Zhou et al. [33], which focused solely on the separation of Sm and Co, this study aims to investigate the separation of Sm, Co, Fe, and Cu with more complex components. Furthermore, this study employed the Taguchi method to determine the priority order of each parameter on precipitation efficiency and determine the optimal precipitation parameters. In comparison to the one-factor-at-a-time experimental method and the full-factor experiment method, the Taguchi method requires fewer experiments to obtain useful statistical information. Therefore, the Taguchi method was adopted for this study.

The efficiency of Sm precipitation is influenced by various factors, such as temperature, the addition of Na₂SO₄, and time [33]. To determine the priority order of these three factors on precipitation efficiency, this study used the Taguchi method. First, the orthogonal array experiment was implemented. This study used a L₉(3⁴) orthogonal table with selected control factors and levels of temperature (70–90 °C), an addition of Na₂SO₄ (6–12 g 100 mL⁻¹), and time (20–60 min), as shown in Table 6. After completing the orthogonal array experiment, this study performed a factor effect analysis to understand the order of priority of each factor affecting the Sm precipitation efficiency and found the preliminary optimal experimental parameters. Finally, this study used the priority ranking of precipitation by each factor to conduct confirmation experiments and obtained the best precipitation parameters.

Table 6. A L₉(3⁴) orthogonal table of Sm precipitation.

No.	Temp.	Time	Na ₂ SO ₄
Unit	°C	min	(w/v)%
1	70	20	6
2	80	40	9
3	90	60	12

3.3.5. Fe and Cu Precipitation

This study examines the precipitation efficiency of Fe, Cu, and Co at different pH values. The results [38] show that Fe precipitation occurs at a pH range of 2–2.7, while Cu precipitation occurs at pH 4.5–6.5, and Co precipitation at pH 7.5–9. Based on these findings, it is believed that adjusting the pH value is an effective method for separating these metals. Furthermore, the research findings [38] indicate that precipitation of each metal can be achieved at room temperature. As a result, this study opted to investigate the precipitation of Fe and Cu at 25 °C.

Given that the parameters that need to be adjusted for Fe and Cu precipitation are pH and time, and based on previous studies [38], it is clear that pH affects metal precipitation more than time. Therefore, the optimal precipitation parameters for Fe and Cu were determined without evaluating the relative importance of each parameter. For Fe precipitation parameter adjustments, the pH range was from 2 to 5 and the time range was from 1 to 30 min. For Cu precipitation parameter adjustments, the pH range was from 5 to 7 and the time range was from 10 to 90 min.

3.3.6. Co Precipitation

To produce a reusable product, this study employed oxalic acid for Co precipitation. For Co precipitation parameter adjustments, the molar ratio ranged from 0.5 to 4, and the time ranged from 1 to 9 min.

3.3.7. Product Preparation and Characterization

To obtain raw materials suitable for magnet production, this study analyzed the oxidation temperature of the precipitate using TGA to confirm the oxidation temperature of each metal. However, sodium samarium bisulfate was not analyzed using TGA due to the generation of sulfur oxides during the analysis process, which could cause damage to the instrument.

After confirming the oxidation temperature of each metal, this study proceeded with the oxidation of the precipitate. Specifically, 5 g of the precipitate was placed into a ceramic vessel, which was put into a high-temperature furnace. The temperature was raised to the required level in order to obtain the oxides of each metal. Finally, the XRD [46] was used to confirm the composition of the product ($\text{NaSm}(\text{SO}_4)_2$, Fe_2O_3 , CuO , and Co_3O_4).

3.3.8. Separation Process

Figure 9 shows the research process. First, this study added sodium sulfate to precipitate Sm from the leachate. The Sm formed a precipitate of $\text{NaSm}(\text{SO}_4)_2$ which was separated from the leachate. Secondly, this study added ammonia to precipitate Fe from the leachate by adjusting the pH, and the Fe formed a $\text{Fe}(\text{OH})_3$ precipitate. Thirdly, this study added ammonia to precipitate Cu by adjusting the pH and obtained a $\text{Cu}(\text{OH})_2$ precipitate. Fourth, the Co was precipitated as CoC_2O_4 by the addition of oxalic acid. Fifth, this study carried out a TGA analysis and calcination experiments to obtain the metal oxides of the precipitates. Finally, this study carried out XRD analysis to confirm the composition of the precipitates.

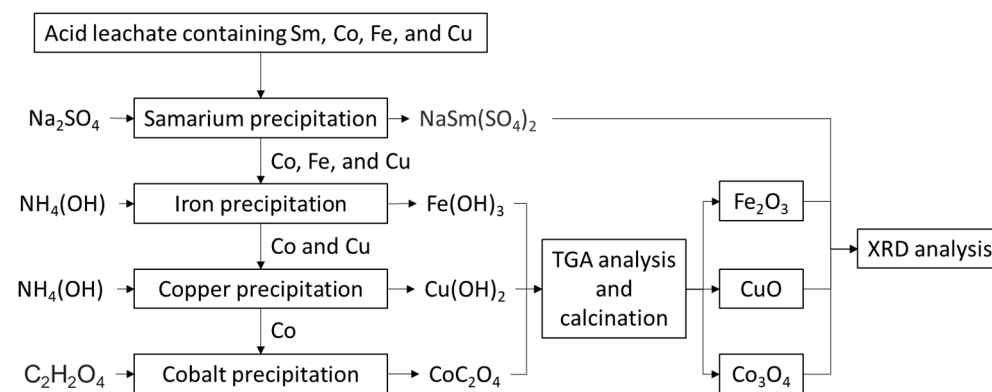


Figure 9. Proposed methodology for recycling Sm, Co, Fe, and Cu.

4. Conclusions

In this study, Na_2SO_4 , NH_4OH , and $\text{H}_2\text{C}_2\text{O}_4$ were used to precipitate and separate Sm, Fe, Cu, and Co. The precipitation efficiencies for Sm, Fe, Cu, and Co were 96.11%, 99.97%, 93.81%, and 98.15%, respectively, with co-precipitation efficiency below 1%. The XRD analysis indicated that the precipitates were $\text{NaSm}(\text{SO}_4)_2$, Fe_2O_3 , CuO , and Co_3O_4 , respectively. This study proposes a new method for recycling SmCo magnets, enabling the recovered metals to be converted back into magnets to support a circular economy.

Compared with solvent extraction and ion exchange techniques, the precipitation method proposed in this study significantly reduces wastewater output and enables a one-step recovery process, thereby streamlining the recovery procedure. Nevertheless, the approach to wastewater treatment in this study warrants further investigation. Given the advanced state of current industrial wastewater treatment technologies, it is anticipated that effective solutions can be implemented to address this aspect with clarity.

Author Contributions: Conceptualization, J.-Z.W.; methodology, J.-Z.W.; validation, J.-Z.W.; investigation, J.-Z.W. and Y.-C.T.; resources, J.-Z.W.; data curation, J.-Z.W.; writing—original draft preparation, J.-Z.W.; writing—review and editing, J.-Z.W. and Y.-C.T.; supervision, Y.-H.S.; project administration, Y.-H.S. All authors have read and agreed to the published version of the manuscript.

Funding: This research received no external funding.

Institutional Review Board Statement: Not applicable.

Informed Consent Statement: Not applicable.

Data Availability Statement: Data is contained within the article.

Acknowledgments: The authors wish to acknowledge the support of the Ministry of Science and Technology, R.O.C.

Conflicts of Interest: Author Yi-Chin Tang was employed by the company China Steel Corporation. The remaining authors declare that the research was conducted in the absence of any commercial or financial relationships that could be construed as a potential conflict of interest.

References

- Golev, A.; Scott, M.; Erskine, P.D.; Ali, S.H.; Ballantyne, G.R. Rare earths supply chains: Current status, constraints and opportunities. *Resour. Policy* **2014**, *41*, 52–59. [[CrossRef](#)]
- Massari, S.; Ruberti, M. Rare earth elements as critical raw materials: Focus on international markets and future strategies. *Resour. Policy* **2013**, *38*, 36–43. [[CrossRef](#)]
- USGS. *Mineral Commodity Summaries 2023*; U.S. Geological Survey: Reston, VA, USA, 2023. [[CrossRef](#)]
- Zhang, L.; Guo, Q.; Zhang, J.; Huang, Y.; Xiong, T. Did China's rare earth export policies work?—Empirical evidence from USA and Japan. *Resour. Policy* **2015**, *43*, 82–90. [[CrossRef](#)]
- Fan, J.H.; Omura, A.; Roca, E. Geopolitics and rare earth metals. *Eur. J. Political Econ.* **2022**, *78*, 102356. [[CrossRef](#)]
- Du, X.; Graedel, T.E. Uncovering the end uses of the rare earth elements. *Sci. Total Environ.* **2013**, *461–462*, 781–784. [[CrossRef](#)]
- Salim, H.; Sahin, O.; Elsayah, S.; Turan, H.; Stewart, R.A. A critical review on tackling complex rare earth supply security problem. *Resour. Policy* **2022**, *77*, 102697. [[CrossRef](#)]
- Wübbecke, J. Rare earth elements in China: Policies and narratives of reinventing an industry. *Resour. Policy* **2013**, *38*, 384–394. [[CrossRef](#)]
- Wang, J.; Guo, M.; Liu, M.; Wei, X. Long-term outlook for global rare earth production. *Resour. Policy* **2020**, *65*, 101569. [[CrossRef](#)]
- Paulick, H.; Machacek, E. The global rare earth element exploration boom: An analysis of resources outside of China and discussion of development perspectives. *Resour. Policy* **2017**, *52*, 134–153. [[CrossRef](#)]
- Li, X.Y.; Ge, J.P.; Chen, W.Q.; Wang, P. Scenarios of rare earth elements demand driven by automotive electrification in China: 2018–2030. *Resour. Conserv. Recycl.* **2019**, *145*, 322–331. [[CrossRef](#)]
- Ascenzi, P.; Bettinelli, M.; Boffi, A.; Botta, M.; Simone, G.D.; Luchinat, C.; Marengo, E.; Mei, H.; Aime, S. Rare earth elements (REE) in biology and medicine. *Rend. Lincei Sci. Fis. E Nat.* **2020**, *31*, 821–833. [[CrossRef](#)]
- Penchoff, D.A.; Sims, C.B.; Windus, T.L. Rare Earth Elements and Critical Materials: Uses and Availability. In *Rare Earth Elements and Actinides: Progress in Computational Science Applications*; Penchoff, D.A., Windus, T.L., Peterson, C.C., Eds.; American Chemical Society: Washington, WA, USA, 2021; pp. 63–74. [[CrossRef](#)]
- Yang, Y.; Lan, C.; Wang, Y.; Zhao, Z.; Li, B. Recycling of ultrafine NdFeB waste by the selective precipitation of rare earth and the electrodeposition of iron in hydrofluoric acid. *Sep. Purif. Technol.* **2020**, *230*, 115870. [[CrossRef](#)]
- Padhan, E.; Nayak, A.K.; Sarangi, K. Recovery of neodymium and dysprosium from NdFeB magnet swarf. *Hydrometallurgy* **2017**, *74*, 210–215. [[CrossRef](#)]
- Padhan, E.; Sarangi, K. Recovery of Nd and Pr from NdFeB magnet leachates with bi-functional ionic liquids based on Aliquat 336 and Cyanex 272. *Hydrometallurgy* **2017**, *167*, 134–140. [[CrossRef](#)]
- Swain, N.; Mishra, S.; Acharya, M.R. Hydrometallurgical route for recovery and separation of samarium (III) and cobalt (II) from simulated waste solution using tri-n-octyl phosphine oxide—A novel pathway for synthesis of samarium and cobalt oxides nanoparticles. *J. Alloys Compd.* **2020**, *815*, 152423. [[CrossRef](#)]
- Pragnell, W.M.; Williams, A.J.; Evans, H.E. The oxidation morphology of SmCo alloys. *J. Alloys Compd.* **2009**, *487*, 69–75. [[CrossRef](#)]
- Su, X.; Wang, Y.; Guo, X.; Dong, Y.; Gao, Y.; Sun, X. Recovery of Sm(III), Co(II) and Cu(II) from waste SmCo magnet by ionic liquid-based selective precipitation process. *Waste Manag.* **2018**, *78*, 992–1000. [[CrossRef](#)]
- Eldosouky, A.; Skulj, I. Recycling of SmCo5 magnets by HD process. *J. Magn. Magn. Mater.* **2018**, *454*, 249–253. [[CrossRef](#)]
- Zheng, X.; Zhang, F.; Liu, E.; Xu, X.; Yan, Y. Efficient Recovery of Neodymium in Acidic System by Free-Standing Dual-Template Docking Oriented Ionic Imprinted Mesoporous Films. *ACS Appl. Mater. Interfaces* **2017**, *9*, 730–739. [[CrossRef](#)]
- Maat, N.; Nachbaur, V.; Larde, R.; Juraszek, J.; Breton, J.M.L. An Innovative Process Using Only Water and Sodium Chloride for Recovering Rare Earth Elements from Nd–Fe–B Permanent Magnets Found in the Waste of Electrical and Electronic Equipment. *ACS Sustain. Chem. Eng.* **2016**, *4*, 6455–6462. [[CrossRef](#)]
- Jha, M.K.; Kumari, A.; Panda, R.; Kumar, J.R.; Yoo, K.; Lee, J.Y. Review on hydrometallurgical recovery of rare earth metals. *Hydrometallurgy* **2016**, *165*, 2–26. [[CrossRef](#)]
- Bogart, J.A.; Cole, B.E.; Boreen, M.A.; Scheluter, E.J. Accomplishing simple, solubility-based separations of rare earth elements with complexes bearing size-sensitive molecular apertures. *Proc. Natl. Acad. Sci. USA* **2016**, *113*, 14887–14892. [[CrossRef](#)] [[PubMed](#)]

25. Walton, A.; Yi, H.; Rowson, N.A.; Speight, J.D.; Mann, V.S.J.; Sheridan, R.S.; Bradshaw, A.; Harris, I.R.; Williams, A.J. The use of hydrogen to separate and recycle neodymium–iron–boron-type magnets from electronic waste. *J. Clean. Prod.* **2015**, *104*, 236–241. [[CrossRef](#)]
26. Moore, M.; Gebert, A.; Stoica, M.; Uhlemann, M.; Loser, W. A route for recycling Nd from Nd-Fe-B magnets using Cu melts. *J. Alloys Compd.* **2015**, *647*, 997–1006. [[CrossRef](#)]
27. Maroufi, S.; Nekouei, R.K.; Sahajwalla, V. Thermal Isolation of Rare Earth Oxides from Nd–Fe–B Magnets Using Carbon from Waste Tyres. *ACS Sustain. Chem. Eng.* **2017**, *5*, 6201–6208. [[CrossRef](#)]
28. Bian, Y.; Guo, S.; Jiang, L.; Liu, J.; Tang, K.; Ding, W. Recovery of Rare Earth Elements from NdFeB Magnet by VIM-HMS Method. *ACS Sustain. Chem. Eng.* **2016**, *4*, 810–818. [[CrossRef](#)]
29. Sinha, M.K.; Pramanik, S.; Kumari, A.; Sahu, S.K.; Prasad, L.B.; Jha, M.K.; Yoo, K.; Pandey, B.D. Recovery of value added products of Sm and Co from waste SmCo magnet by hydrometallurgical route. *Sep. Purif. Technol.* **2017**, *179*, 1–12. [[CrossRef](#)]
30. Orefice, M.; Audoor, H.; Li, Z.; Binnemans, K. Solvometallurgical route for the recovery of Sm, Co, Cu and Fe from SmCo permanent magnets. *Sep. Purif. Technol.* **2019**, *219*, 281–289. [[CrossRef](#)]
31. Xu, T.; Zhang, X.; Lin, Z.; Lu, B.; Ma, C.; Gao, X. Recovery of rare earth and cobalt from Co-based magnetic scraps. *J. Rare Earths* **2010**, *28*, 485–488. [[CrossRef](#)]
32. Sahoo, K.; Nayak, A.K.; Ghosh, M.K.; Sarangi, K. Preparation of Sm₂O₃ and Co₃O₄ from SmCo magnet swarf by hydrometallurgical processing in chloride media. *J. Rare Earths* **2018**, *36*, 725–732. [[CrossRef](#)]
33. Zhou, K.; Wang, A.; Zhang, D.; Zhang, X.; Yang, T. Sulfuric acid leaching of SmCo alloy waste and separation of samarium from cobalt. *Hydrometallurgy* **2017**, *174*, 66–70. [[CrossRef](#)]
34. Wang, J.Z.; Tang, Y.C.; Shen, Y.H. Leaching of Sm, Co, Fe, and Cu from Spent SmCo Magnets Using Organic Acid. *Metals* **2023**, *13*, 233. [[CrossRef](#)]
35. Torkaman, R.; Moosavian, M.A.; Mostaedi, M.T.; Safdari, J. Solvent extraction of samarium from aqueous nitrate solution by Cyanex301 and D2EHPA. *Hydrometallurgy* **2013**, *137*, 101–107. [[CrossRef](#)]
36. Wang, J.Z.; Hsieh, Y.H.; Tang, Y.C.; Shen, Y.H. Separation of Cobalt, Samarium, Iron, and Copper in the Leaching Solution of Scrap Magnets. *Metals* **2023**, *13*, 90. [[CrossRef](#)]
37. Onoda, H.; Kurioka, Y. Selective removal and recovery of samarium from mixed transition metal solution using phosphoric acid. *J. Environ. Chem. Eng.* **2016**, *4*, 4536–4539. [[CrossRef](#)]
38. Monhemius, J. Precipitation diagrams for metal hydroxides, sulphides, arsenates and phosphates. *Trans. Inst. Min. Metall.* **1977**, *86*, C202–C206. Available online: https://www.researchgate.net/publication/266137129_Precipitation_diagrams_for_metal_hydroxides_sulphides_arsenates_and_phosphates (accessed on 28 August 2023).
39. Fan, E.; Yang, J.; Huang, Y.; Lin, J.; Arshad, F.; Wu, F.; Li, L.; Chen, R. Leaching Mechanisms of Recycling Valuable Metals from Spent Lithium-Ion Batteries by a Malonic Acid-Based Leaching System. *ACS Appl. Energy Mater.* **2020**, *3*, 8532–8542. [[CrossRef](#)]
40. Li, L.; Fan, E.; Guan, Y.; Zhang, X.; Xue, Q.; Wei, L.; Wu, F.; Chen, R. Sustainable Recovery of Cathode Materials from Spent Lithium-Ion Batteries Using Lactic Acid Leaching System. *ACS Sustain. Chem. Eng.* **2017**, *5*, 5224–5233. [[CrossRef](#)]
41. Ackermann, S.; Lazic, B.; Armbruster, T.; Doyle, S.; Grevel, K.D.; Majzlan, J. Thermodynamic and crystallographic properties of kornelite [Fe₂(SO₄)₃·~7.75H₂O] and paracoquimbite [Fe₂(SO₄)₃·9H₂O]. *Am. Mineral.* **2009**, *94*, 1620–1628. [[CrossRef](#)]
42. Majzlan, J.; Botez, C.; Stephens, P.W. The crystal structures of synthetic Fe₂(SO₄)₃(H₂O)₅ and the type specimen of lausenite. *Am. Mineral.* **2005**, *90*, 411–416. [[CrossRef](#)]
43. Majzlan, J.; Navrotsky, A.; McCleskey, R.B.; Alpers, C.N. Thermodynamic properties and crystal structure refinement of ferricopiapite, coquimbite, rhomboclase, and Fe₂(SO₄)₃(H₂O)₅. *Eur. J. Mineral.* **2006**, *18*, 175–186. [[CrossRef](#)]
44. Denisenko, Y.G.; Sedykh, A.E.; Basova, S.A.; Atuchin, V.V.; Molokeev, M.S.; Aleksandrovsky, A.S.; Krylov, A.S.; Oreshonkov, A.S.; Khritokhin, N.A.; Salnikova, E.I.; et al. Exploration of the structural, spectroscopic and thermal properties of double sulfate monohydrate NaSm(SO₄)₂·H₂O and its thermal decomposition product NaSm(SO₄)₂. *Adv. Powder Technol.* **2021**, *32*, 3943–3953. [[CrossRef](#)]
45. Deng, Y.; Zhang, Y.; Ding, Y. Recovery of rare earths in different media with novel dicarboxylate based ionic liquid and application to recycle SmCo magnets. *Hydrometallurgy* **2022**, *210*, 105844. [[CrossRef](#)]
46. Wang, J.Z.; Lin, H.H.; Tang, Y.C.; Shen, Y.H. Recovery of Calcium from Reaction Fly Ash. *Sustainability* **2023**, *15*, 2428. [[CrossRef](#)]

Disclaimer/Publisher’s Note: The statements, opinions and data contained in all publications are solely those of the individual author(s) and contributor(s) and not of MDPI and/or the editor(s). MDPI and/or the editor(s) disclaim responsibility for any injury to people or property resulting from any ideas, methods, instructions or products referred to in the content.